Available online at www.sciencedirect.com
SCIENCE DIRECT®
Journal of Power Sources 132 (2004) 156–160
JOURNAL OF POWER SOURCES
www.elsevier.com/locate/jpowsour

# Relationship between the electrochemical and particle properties of $LiMn_2O_4$ prepared by ultrasonic spray pyrolysis

K. Matsuda, I. Taniguchi*

*Department of Chemical Engineering, Graduate School of Science and Engineering, Tokyo Institute of Technology, 2-12-1, Ookayama, Meguro-ku, Tokyo 152-8552, Japan*

Received 22 September 2003; accepted 5 January 2004

**Abstract**

Spinel $LiMn_2O_4$ particles were successfully synthesized by an ultrasonic spray pyrolysis method from the precursor solutions; various combinations of nitrate, acetates or formats of lithium and manganese were stoichiometrically dissolved in distilled water. The product characteristics, such as crystallinity, specific surface area, particle morphology and interior structure of particles, were examined with X-ray diffraction (XRD), the Brunauer–Emmet–Teller (BET) method, field emission scanning electron microscopy (FE-SEM) and transmission electron microscopy (TEM). All the samples exhibited a pure cubic spinel structure without any impurities in the XRD patterns, while the surface morphology of as-prepared powders was classified into four patterns and the interior structure three patterns.

The as-prepared samples were then used as cathode active materials for lithium-ion battery, and electrochemical studies were carried out on the charge/discharge characteristics of the Li/$LiMn_2O_4$ cells. The effect of $LiMn_2O_4$ particle properties such as crystallite size, specific surface area and particle morphology on the electrochemical properties were also discussed in details.


*Keywords:* $LiMn_2O_4$; Spray pyrolysis; Particle properties; Lithium batteries; Cathode materials

## 1. Introduction

The lithium-ion batteries have been widely adopted as the most promising portable energy source in electronic products such as lap top computers and cellular telephones because of their high working voltage, high energy density, and good cycleability. These batteries, consisting of lithium intercalation compounds as positive electrode, graphite or carbon as negative electrode and an organic electrolyte, are under consideration for the electric vehicle and the hybrid electric vehicle application. In these batteries, the most recent candidates as cathode materials are a family of lithium transition metal oxides such as $LiCoO_2$, $LiNiO_2$, or $LiMn_2O_4$. Among these cathode materials, $LiCoO_2$ is now commercially used, but is very expensive. Thus, $LiNiO_2$ and $LiMn_2O_4$ are now studied extensively as substitutes for $LiCoO_2$. Nickel is cheaper than cobalt, and the theoretical capacity of $LiNiO_2$ is very high, however, it is difficult to prepare the material. $LiMn_2O_4$ is cheap and easy to prepare, but there is a problem of capacity fading during charge/discharge cycle in the material [1–3]. Therefore, the urgent research target for the latter material is to decrease the capacity fading.

So far, it has been suggested that the capacity fading is due to the decomposition of electrolyte at high-voltage region, the dissolution of $Mn^{3+}$ ions into the electrolyte, and/or the Jahn–Teller distortion [3–6]. However, Huang et al. [7] have recently reported that the cycle characteristic is affected by the particle properties such as morphology and crystallites of particles. It has also been reported by Aikiyo et al. [8] that the cycleability of $LiMn_2O_4$ prepared by spray pyrolysis method are affected by the particles morphology.

In our previous papers [9–11], it has been reported that the spinel $LiMn_2O_4$ powders could be easily prepared by ultrasonic spray pyrolysis method and their particle properties such as particle morphology, crystallite size, and specific surface area, were easily controlled by this preparation method, in comparison with other preparation methods [4,12–15]. In this work, we synthesized $LiMn_2O_4$ samples using an ultrasonic spray pyrolysis method from various precursor solutions, examined their particles properties and electrochemical properties, and finally discussed the relationship between the particles and electrochemical properties of the $LiMn_2O_4$ particles.

* Corresponding author. Tel.: +81-3-5734-2155; fax: +81-3-5734-2155.
*E-mail address:* itaniguc@chemeng.titech.ac.jp (I. Taniguchi).

0378-7753/$ – see front matter © 2004 Elsevier B.V. All rights reserved.
doi:10.1016/j.jpowsour.2004.01.019

## 2. Experimental

Precursor solutions were prepared by dissolving a stoichiometric ratio of Li-salt ($LiNO_3$, $Li(CH_3COO)\cdot 2H_2O$ or $Li(HCOO)\cdot H_2O$) and Mn-salt ($Mn(NO_3)_2\cdot 6H_2O$, $Mn(HCOO)_2\cdot 2H_2O$ or $Mn(CH_3COO)_2\cdot 4H_2O$) in a distilled water. The total concentration of metal ion was $[Li^{1+}] + [Mn^{2+}] = 0.54\,mol/dm^3$, while the solution with mixtures of the metal cations always had an atomic ratio of $Li/Mn = 1/2$.

A schematic diagram of the experimental apparatus have been described elsewhere [9–11]. It consists of an ultrasonic nebulizer (1.7 MHz, Omron Co. Ltd., Model NE-U12), a laminar flow aerosol reactor (a high quality ceramic tube of 20-mm inner diameter and 1105 mm length) and an electrostatic precipitator. The precursor solution was atomized at a frequency of 1.7 MHz by the ultrasonic nebulizer. The sprayed droplets were carried to the reactor, heated by an electric furnace at 1073 K, by air and converted into solid oxide particles through the process of evaporation of a solvent, precipitation of solute, drying, pyrolysis and sintering within the laminar flow aerosol reactor. The resulting particles were collected at the reactor exit by the electrostatic precipitator [16] at 423 K, while the gasses were dried and cleaned up by passing them through a cold trap. The air flow rate was varied from 0.5 to 4 $dm^3$/min.

The crystalline phase of as-prepared powders was examined by X-ray diffraction (XRD, Phillips, PW1700) with a scan speed of 2.4°/min for crystal analysis ranging from 4° to 70° and 0.6°/min for the lattice parameter measurements ranging from 40° to 90°, respectively. The average size of crystallites was estimated using Scherrer's formula. The particle morphology was examined by field-emission scanning electron microscopy (FE-SEM, Hitachi, S-800) operated at 15 kV. The geometric mean diameter and geometric standard deviation were determined by randomly sampling around 500 particles from the SEM pictures. The interior structure of as-prepared particles was observed by using transmission electron microscopy (TEM, JEOL Ltd., JEM-200CX), and the specific surface area was determined by BET method (Shimazu Co., FlowSorb II 2300). The chemical composition of as-prepared powders was checked by inductively coupled plasma spectroscopy (ICP-AES, Seiko Instruments Inc., SPS1500VR). The average oxidation state of Mn was determined by a redox titration method with potassium permanganate $KMnO_4$.

The electrochemical characterization of as-prepared powders was examined at room temperature in a half-cell configuration, Li metal/electrolyte 1 $mol/dm^3$ $LiClO_4$-propylene carbonate (PC)/cathode material. The cathode materials consist of $LiMn_2O_4$ powders, acetylene black (AB) as conductor and polytetrafluoroethylene (PTFE) as binder in the ratio of 75:20:5 by weight. These were dried at 373 K for 24 h in a vacuum oven. The charge and discharge characteristics of the cathode were evaluated at current densities of 0.2 $mA/cm^2$ or 0.5 in the range 3.5–4.4 V versus $Li/Li^+$. All electrochemical measurements were conducted at room temperature in a glove box filled with high purity argon gas (99.9995%).

## 3. Results and discussion

Spinel $LiMn_2O_4$ particles were successfully synthesized by an ultrasonic spray pyrolysis method from the precursor solutions; various combinations of nitrate, acetates or formats of lithium and manganese were stoichiometrically dissolved in distilled water. From the SEM and TEM pictures of as-prepared $LiMn_2O_4$ particles, the surface structure of resulting $LiMn_2O_4$ particles were classified into four patterns: (A) porous surface structure(run nos. 1–6), (B) hybrid structure with both porous and smooth surface (run nos. 7–9), (C) smooth surface structure (run nos. 10 and 11), and (D) shrinkage surface structure (run nos. 12 and 13), while the interior structure of resulting particles were classified into three patterns: (E) dense structure (run nos. 1–6), (F) hollow structure with thicker shell (run nos. 7–9, 12 and 13), and (G) hollow structure with thinner shell (run nos. 10 and 11). However, all the samples were a secondary particle that was formed by the cohesion of the primary particles with around a few ten nanometer sizes. The XRD patterns of all the samples were identified a single-phase spinel with a space group *Fd*3*m* in which the lithium ions occupy the tetrahedral (8a) sites and manganese metal ions reside at the octahedral (16d) sites. Fig. 1 shows some examples of the XRD patterns, SEM and TEM photographs of $LiMn_2O_4$ particles prepared from various precursor solutions.

The particle properties of as-prepared particles are also summarized in Table 1. The determined lattice parameters and chemical composition of all the samples show in good agreement with the theoretical ones, respectively. Except for the specific surface area and crystallite size, the particles properties of samples were quite similar.

Fig. 2 shows the first charge-discharge curves of the $Li|LiMn_2O_4$ cell. The dense $LiMn_2O_4$ particles with porous microstructure, as shown in the figure, were used as the cathode active materials in the cell. The cell was initially charged at a rate of 0.2 $mA/cm^2$ to upper limit of 4.4 V. Upon discharge, the lower potential limit was 3.5 V. It can be seen clearly that the charge/discharge curves of the samples with various crystallite sizes of $LiMn_2O_4$ particles had two voltage plateaus, which is a remarkable characteristic of a well-defined $LiMn_2O_4$ spinel. The initial discharge capacity of run nos. 2, 4 and 5 is 120, 117 and 110 mAh/g, respectively. The initial discharge capacity of the cells increases with the crystallite size of $LiMn_2O_4$ particles at the same morphology and specific surface area of the particles. The variation of discharge capacity of the $Li|LiMn_2O_4$ cells with number of cycles is presented in Fig. 3. The dense $LiMn_2O_4$ particles with porous microstructure, as shown in the figure, were also used as the cathode active materials. The ordinate of the figure represents the discharge capacity normalized by the theoretical one (148 mAh/g). The nor-

Table 1
Particle properties of as-prepared $LiMn_2O_4$ powders

| Run no. | Combination of precursor | Gas flow rate ($dm^3$/min) | Geometric mean diameter (μm) | Geometric standard deviation | Chemical composition | | | Mn's average valent | Lattice parameter (Å) | Crystallite size (nm) | Specific surface area ($m^2$/g) |
|---|---|---|---|---|---|---|---|---|---|---|---|
| | | | | | Li | Mn | O | | | | |
| 1 | $LiNO_3$–$Mn(NO_3)_2{\cdot}6H_2O$ | 0.5 | 0.854 | 1.43 | 1.00 | 1.99 | 4.02 | 3.54 | 8.2416 | 18.84 | 10.92 |
| 2 | $Li(HCOO){\cdot}H_2O$–$Mn(NO_3)_2{\cdot}6H_2O$ | 0.5 | 0.852 | 1.46 | 1.00 | 1.99 | 3.96 | 3.47 | 8.2481 | 24.97 | 13.11 |
| 3 | $LiNO_3$–$Mn(NO_3)_2{\cdot}6H_2O$ | 1 | 0.870 | 1.44 | 1.00 | 2.04 | 4.11 | 3.54 | 8.2417 | 18.54 | 13.25 |
| 4 | $Li(HCOO){\cdot}H_2O$–$Mn(NO_3)_2{\cdot}6H_2O$ | 1 | 0.982 | 1.48 | 1.00 | 1.94 | 3.88 | 3.48 | 8.2455 | 22.35 | 13.32 |
| 5 | $Li(CH_3COO){\cdot}2H_2O$–$Mn(NO_3)_2{\cdot}6H_2O$ | 1 | 0.871 | 1.42 | 1.00 | 1.96 | 3.91 | 3.48 | 8.2399 | 19.00 | 13.89 |
| 6 | $Li(CH_3COO){\cdot}2H_2O$–$Mn(NO_3)_2{\cdot}6H_2O$ | 4 | 0.983 | 1.44 | 1.00 | 1.95 | 3.94 | 3.53 | 8.2420 | 17.41 | 17.54 |
| 7 | $Li(HCOO){\cdot}H_2O$–$Mn(HCOO)_2{\cdot}2H_2O$ | 1 | 1.046 | 1.41 | 1.00 | 1.96 | 3.90 | 3.47 | 8.2432 | 21.52 | 10.20 |
| 8 | $Li(CH_3COO){\cdot}2H_2O$–$Mn(HCOO)_2{\cdot}2H_2O$ | 1 | 0.940 | 1.45 | 1.00 | 1.99 | 3.96 | 3.48 | 8.2467 | 17.66 | 10.21 |
| 9 | $Li(CH_3COO){\cdot}2H_2O$–$Mn(HCOO)_2{\cdot}2H_2O$ | 2 | 0.957 | 1.44 | 1.00 | 2.03 | 3.98 | 3.43 | 8.2416 | 14.61 | 10.19 |
| 10 | $Li(HCOO){\cdot}H_2O$–$Mn(CH_3COO)_2{\cdot}4H_2O$ | 1 | 1.079 | 1.43 | 1.00 | 1.97 | 3.97 | 3.53 | 8.2436 | 18.68 | 14.24 |
| 11 | $Li(CH_3COO){\cdot}2H_2O$–$Mn(CH_3COO)_2{\cdot}4H_2O$ | 1 | 1.044 | 1.37 | 1.00 | 1.94 | 3.90 | 3.50 | 8.2432 | 17.75 | 13.40 |
| 12 | $LiNO_3$–$Mn(HCOO)_2{\cdot}2H_2O$ | 1 | 0.922 | 1.44 | 1.00 | 1.97 | 3.97 | 3.52 | 8.2452 | 25.75 | 10.62 |
| 13 | $LiNO_3$–$Mn(HCOO)_2{\cdot}2H_2O$ | 4 | 1.022 | 1.44 | 1.00 | 2.02 | 4.07 | 3.53 | 8.2416 | 17.82 | 12.44 |

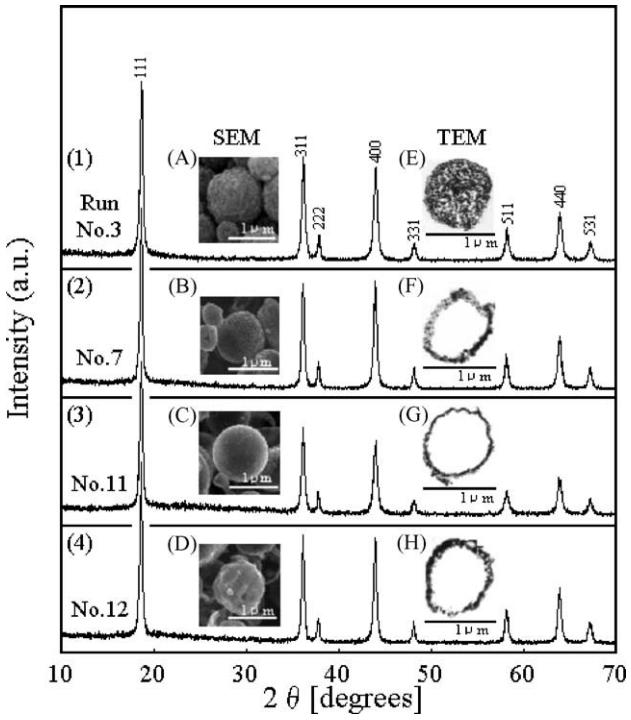


Fig. 1. Some examples of XRD patterns, SEM and TEM photographs of $LiMn_2O_4$ particles prepared from various precursor solutions; (1) dense $LiMn_2O_4$ particles with porous surface structure (run nos. 1–6), (2) hollow $LiMn_2O_4$ particles with hybrid surface structure (run nos. 7–9), (3) hollow $LiMn_2O_4$ particles with smooth surface structure (run nos. 10 and 11), (4) hollow $LiMn_2O_4$ particles with shrinkage surface structure.

malized discharge capacity decreases with the crystallite size of $LiMn_2O_4$ particles in each number of cycles. It is clearly evident from Figs. 2 and 3 that the electrochemical property of $LiMn_2O_4$ particles prepared by spray pyrolysis

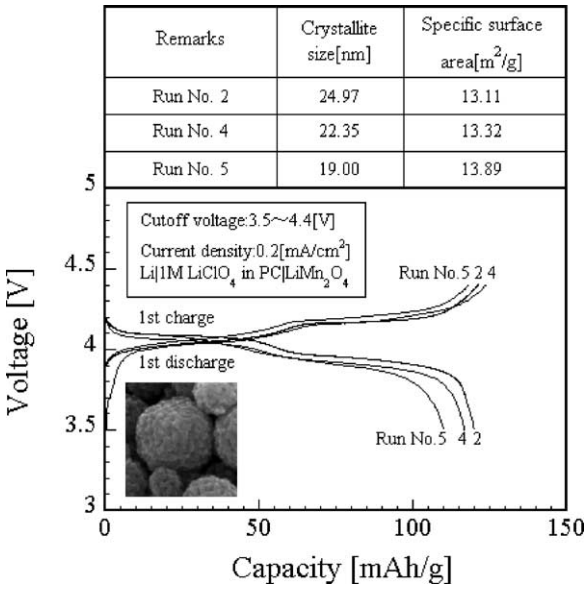


Fig. 2. Some examples of first charge–discharge curves of $Li|LiMn_2O_4$ cells. Voltage range 3.5–4.4 V with a constant current density of 0.2 $mA/cm^2$.

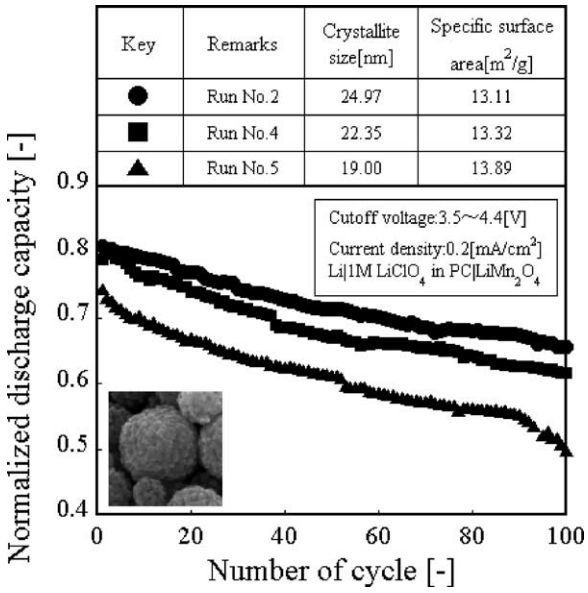


Fig. 3. Effect of crystallite size of $LiMn_2O_4$ particles on cycle performance. Voltage range 3.5–4.4 V with a constant current density of 0.2 mA/cm$^2$.

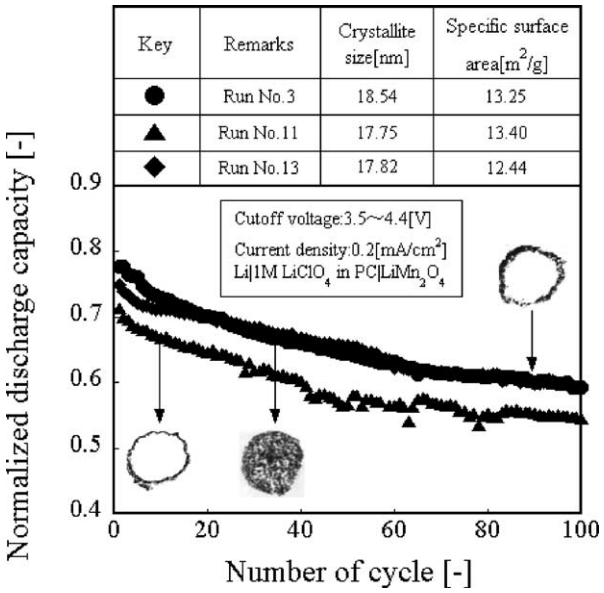


Fig. 5. Effect of interior structure of $LiMn_2O_4$ particles on cycle performance. Voltage range 3.5–4.4 V with a constant current density of 0.2 mA/cm$^2$.

is significantly affected by the crystallite size of $LiMn_2O_4$ particles. The larger crystallite size, the smaller capacity fading.

Fig. 4 shows the variation of discharge capacity of the Li|$LiMn_2O_4$ cells with number of cycles; the $LiMn_2O_4$ particles with various specific surface area were used as cathode active materials in the cell. It can be clearly seen that the smaller specific surface area, the better cycle performance. This fact may indicate that the large specific surface area of $LiMn_2O_4$ particles promotes the Mn dissolution into the electrolyte.

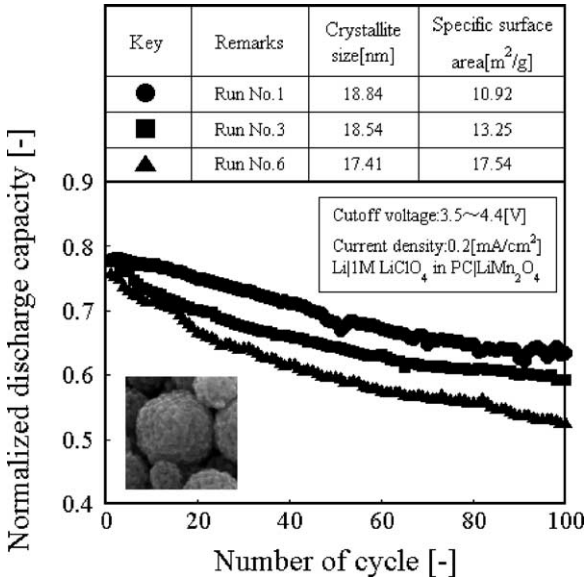


Fig. 4. Effect of specific surface area of $LiMn_2O_4$ particles on cycle performance. Voltage range 3.5–4.4 V with a constant current density of 0.2 mA/cm$^2$.

Fig. 5 shows the variation of discharge capacity of the Li|$LiMn_2O_4$ cells with number of cycles; various $LiMn_2O_4$ particles: (E) dense structure, (F) hollow structure with thicker shell and (G) hollow structure with thinner shell were used as cathode active materials in the cells. All the samples are similar on the specific surface area and crystallite size of $LiMn_2O_4$ particles. The cycle performance for dense $LiMn_2O_4$ particles were similar to that for the hollow $LiMn_2O_4$ particles with thicker shell, while the capacity fading for the hollow $LiMn_2O_4$ particles with thinner shell become considerable with number of cycles. In our previous work [11], from the SEM observation of cathode after 100 cycles, the dense $LiMn_2O_4$ particles and the hollow $LiMn_2O_4$ particles with thicker shell kept mostly their original structure after the cycle. However, the hollow $LiMn_2O_4$ particles with thinner shell were broken after the cycle. This may cause to the capacity fading for the hollow $LiMn_2O_4$ particles with thinner shell.

Fig. 6 shows the cycle performance of the Li|$LiMn_2O_4$ cells; the $LiMn_2O_4$ particles synthesized from various precursor solutions were used as cathode active materials in the cells, however the specific surface area and crystallite size of the as-prepared particles were quite similar in each particle structure ((A) dense $LiMn_2O_4$ particles and (C) hollow $LiMn_2O_4$ particles with thinner shell). In each particle structure, the cycle behavior is quite similar. It may be clearly seen that the electrochemical properties of $LiMn_2O_4$ prepared by ultrasonic spray pyrolysis are only affected by the interior structure, specific surface area and crystallite size of $LiMn_2O_4$ particles.

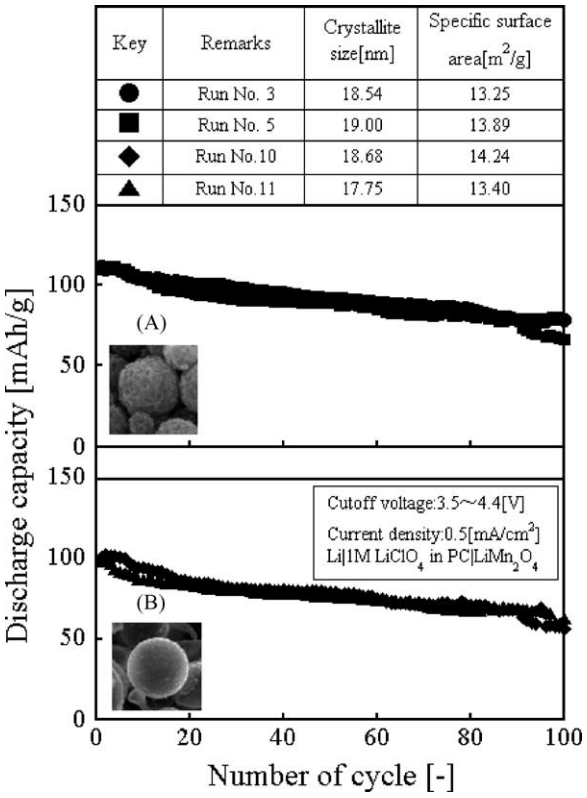


Fig. 6. Cycle performance of $LiMn_2O_4$ particles with same particle properties synthesized from various precursor solutions: (A) dense $LiMn_2O_4$ particles, (B) hollow $LiMn_2O_4$ particles with thinner shell. Voltage range 3.5–4.4 V with a constant current density of 0.5 mA/cm$^2$.

## 4. Conclusions

The spinel $LiMn_2O_4$ powders were prepared by using an ultrasonic spray pyrolysis method from various precursor solutions. From the SEM and TEM pictures of as-prepared samples, the surface structure of resulting $LiMn_2O_4$ particles were classified into four patterns and the interior structure three patterns. However, all the samples had the spinel structure, and the determined lattice parameter and chemical composition of all the samples showed good agreement with the theoretical ones, respectively.

To investigate the electrochemical characteristics of as-prepared $LiMn_2O_4$ particles, the fabrication of Li|$LiMn_2O_4$ cells was made and the cycle performance were evaluated galvanostatically at room temperature. As the results, the smaller specific surface area and the larger crystallite size, the better cycle performance. The dense $LiMn_2O_4$ particles were also suitable for the cathode active material of lithium ion battery. It could be seen clearly that the interior structure, specific surface area and crystallite size of $LiMn_2O_4$ played a key part in the electrochemical properties of $LiMn_2O_4$ particles prepared by ultrasonic spray pyrolysis.

## Acknowledgements

This research work has been partially supported by the Ministry of Education, Culture and Science of Japan (Grant No. 11650774).

## References

[1] J.M. Tarascon, W.R. McKinnon, F. Coowar, T.N. Bowmer, G. Amatucci, D. Guyomard, J. Electrochem. Soc. 141 (1994) 1421.
[2] R.J. Gummow, A. de Kock, M.M. Thackeray, Solid State Ionics 69 (1994) 59.
[3] Y. Xia, Y. Zhou, M. Yoshio, J. Electrochem. Soc. 144 (1997) 2593.
[4] J.M. Tarascon, E. Wang, F.K. Shokoohi, W.R. McKinnon, S. Colson, J. Electrochem. Soc. 138 (1991) 2859.
[5] A. Yamada, M. Tanaka, Mater. Res. Bull. 30 (1995) 715.
[6] A. Yamada, J. Solid State Chem. 122 (1995) 160.
[7] H. Huang, C.H. Chen, R.C. Perego, E.M. Kelder, L. Chen, J. Schoonman, Solid State Ionics 127 (2000) 31.
[8] H. Aikiyo, K. Nakane, N. Ogata, T. Ogihara, J. Ceram. Soc. Jpn. 109 (2001) 506.
[9] I. Taniguchi, C.K. Lim, Kagaku Kogaku Ronbunshu 27 (2001) 93.
[10] I. Taniguchi, C.K. Lim, D. Song, M. Wakihara, Solid State Ionics 146 (2002) 239.
[11] K. Matsuda, I. Taniguchi, Kagaku Kogaku Ronbunshu 29 (2003) 232.
[12] M. Yoshio, H. Noguchi, H. Nakamura, Y. Xia, H. Takeshige, K. Ikeda, Electrochemistry 63 (1995) 941.
[13] X. Qui, X. Sun, W. Shen, N. Chen, Solid State Ionics 93 (1997) 335.
[14] Y.K. Sun, I.H. Oh, K.Y. Kim, Ind. Eng. Chem. Res. 36 (1997) 4839.
[15] K.T. Hwang, W.S. Um, H.S. Lee, J.K. Song, K.W. Chung, J. Power Sources 74 (1998) 169.
[16] K. Okuyama, M. Shimada, M. Adachi, N. Tohge, J. Aerosol Sci. 24 (1993) 357.